ACS APPLIED MATERIALS & INTERFACES

Letter

www.acsami.org

Bioinspired Air-Retaining Nanofur for Drag Reduction

Maryna N. Kavalenka,* Felix Vüllers, Simone Lischker, Claudia Zeiger, Andreas Hopf, Michael Röhrig, Bastian E. Rapp, Matthias Worgull, and Hendrik Hölscher*

Institute for Microstructure Technology, Karlsruhe Institute of Technology (KIT), Hermann-von-Helmholtz-Platz 1, 76344 Eggenstein-Leopoldshafen, Germany

ABSTRACT: Bioinspired nanofur, covered by a dense layer of randomly distributed high aspect ratio nano- and microhairs, possesses superhydrophobic and air-retaining properties. Nanofur is fabricated using a highly scalable hot pulling method in which softened polymer is elongated with a heated sandblasted plate. Here we investigate the stability of the underwater air layer retained by the irregular nanofur topography by applying hydraulic pressure to the nanofur kept underwater, and evaluate the gradual changes in the air-covered area. Furthermore, the drag reduction resulting from the nanofur air retention is characterized by measuring the pressure drop across channels with and without nanofur.

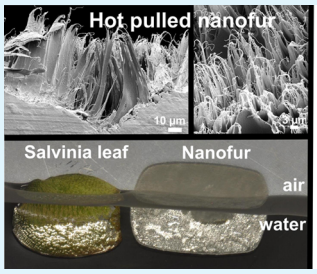

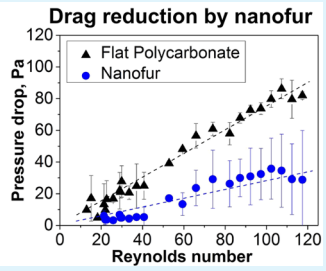

KEYWORDS: *drag reduction, air retention, superhydrophobic, bioinspired, wetting transition*

Natural micro- and nanostructured surfaces and their exceptional properties inspire the development of new technologies and often provide solutions for improving existing ones, such as developing technical surfaces with enhanced thermal, mechanical and optical properties, self-cleaning ability, and surfaces which reduce frictional drag.[1−4] In recent years, drag reduction research has received considerable attention, in large part because it can help to reduce the enormous fuel consumption by international shipping, which increased from 64.5 million metric tons in 1950 to 280 million in 2001.[5] In marine vessels, more than half of the energy used for propulsion is wasted on overcoming surface friction. The same problem exists in transporting liquids through pipes, where the pumps work mainly to overcome the pipe wall friction.[6] In nature, water-repelling surfaces of floating plants and semiaquatic insects allow them to effectively move on and in water, and breathe while submerged underwater.[7,8] These properties result from the ability of some natural superhydrophobic surfaces to passively fix and retain an air film underwater, thus reducing the solid surface area in contact with water. Superhydrophobic and air-retaining properties of natural surfaces often originate from the dense layers of micro- and nanoscale hairs covering them, as on the surfaces of the water bug *Notonecta glauca*[9,10] and the water fern *Salvinia*.[11] Superhydrophobicity of these surfaces is described by a Cassie−Baxter wetting state, in which the tips of the micro- and nanohairs support the water and help to trap the air between the structures. It is characterized by high contact angles (>150°) and low contact angle hysteresis.[7] The underwater air film minimizes the water−solid contact area and, therefore, significantly reduces the frictional drag between water and solid.

Artificial superhydrophobic surfaces are obtained by fabricating micro- and nanostructures on materials with low surface energy, and have been shown to reduce frictional drag.[12−16] The major problem of the air-retaining surfaces is the instability of the retained air under external stimuli such as pressure, flow, impact or vibration.[17−19] When water replaces air between the micro- and nanostructures, the surface looses its superhydrophobic and drag reduction properties. Despite the reported drag reduction achieved by artificial surfaces, the instability of their air layer results in a limited operation time and conditions.[11,14,19] Contrarily, *Salvinia* and *Notonecta glauca* can sustain the underwater air layer for a long time (days to months).[11,20,21]

In this paper, we investigate the air-retaining and drag reduction properties of a bioinspired nanofur material with complex topography. Similar to the air-retaining surfaces of *Salvinia* fern and *Notonecta glauca* bug, our nanofur surface is covered by a dense layer of randomly distributed high aspect ratio nano- and microhairs with microcavities between them. Such topography of the nanofur satisfies the requirements necessary for stable air retention.[22] Superhydrophobic nanofur is fabricated using a highly scalable hot pulling method in which softened viscous polymer is locally elongated with a heated sandblasted steel plate due to adhesion to the sandblasted surface.[23,24] The stability of the underwater air layer retained by nanofur is studied by applying hydraulic pressure to the nanofur kept underwater, and then the experimental results are compared to the theoretical prediction. To study the drag reduction properties resulting from the air-retention, we measure the pressure drop across microchannels in which nanofur serves as a channel wall and channels without nanofur.

Received: February 26, 2015
Accepted: May 6, 2015
Published: May 6, 2015

DOI: 10.1021/acsami.5b01772
ACS Appl. Mater. Interfaces 2015, 7, 10651−10655

The nanofur shown in scanning electron microscopy (SEM) images in Figure 1A, B was fabricated from polycarbonate

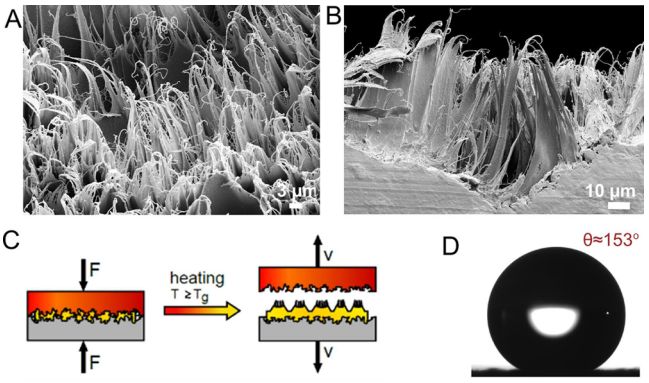

Figure 1. Nanofur fabricated on the polymer surface is inspired by hair-covered surfaces of plants and insects. (A) SEM images of the nanofur fabricated from polycarbonate. The tips of the hairs are less than 200 nm in diameter. (B) Cross-sectional SEM image of the nanofur reveals that hairs are tens of microns long. (C) Schematic of the hot pulling technique with a heated sandblasting steel plate used for nanofur fabrication. (D) Photograph of the water droplet on the superhydrophobic nanofur surface with contact angle $\theta \approx 153°$.

(Makrolon LED2045, Bayer, Germany) using a hot pulling technique. A schematic of the hot pulling technique is illustrated in Figure 1C. Hot pulling is a modified hot embossing process, in which high demolding forces occurring during the polymer and mold separation are used to create high-aspect-ratio nano- and microstructures.[23−27] The greatest advantage of the hot pulling method is that it uses a sandblasted steel plate instead of the expensive microstructured molds used in hot embossing. The plate is patterned by sandblasting it with aluminum silicate clinker (0.6−1.4 mm), and then with aluminum oxide abrasive 53 ± 3 μm). A hot embossing machine (Jenoptik, Germany) is used for hot pulling. The sandblasted plate is heated above the glass transition temperature of the polycarbonate (T_g = 144 °C) and pressed into the material attached to the bottom plate using following parameters: T = 215 °C, embossing velocity 0.4 mm/min, penetration depth 200 μm. Softened polycarbonate fills the cavities of the mold, which is then retracted with 0.3 mm/min velocity. Mold retraction results in polymer elongation and creates a cratered surface densely covered with nanohairs, as shown in Figure 1A. A cross-sectional SEM image of the nanofur is shown in Figure 1B. The hierarchical nanohairs are tens of micrometers long with tips of less than 200 nm in diameter and a typical density ranging from 90 000 to 150 000 hairs/mm^2, as was estimated from SEM images by counting the topmost nanohairs.[24]

The resulting nanofur is superhydrophobic with contact angles above 150° (Figure 1D). The surface of the nanofur has similar properties to the natural air-retaining surfaces of the *Salvinia* fern and the *Notonecta glauca* water bug. When nanofur is submerged underwater, air locked between its nano- and microhairs forms an air film on the surface. An optical image of the nanofur sheet and the *Salvinia Molesta* leaf partially submerged underwater is shown in Figure 2A. Silvery layers visible on both the nanofur and the plant leaf underwater are the result of the light reflection at the air−water interface, and indicate the air trapped by these hair-covered surfaces. Solga et al.,[22] after analyzing natural air-retaining surfaces of plants and

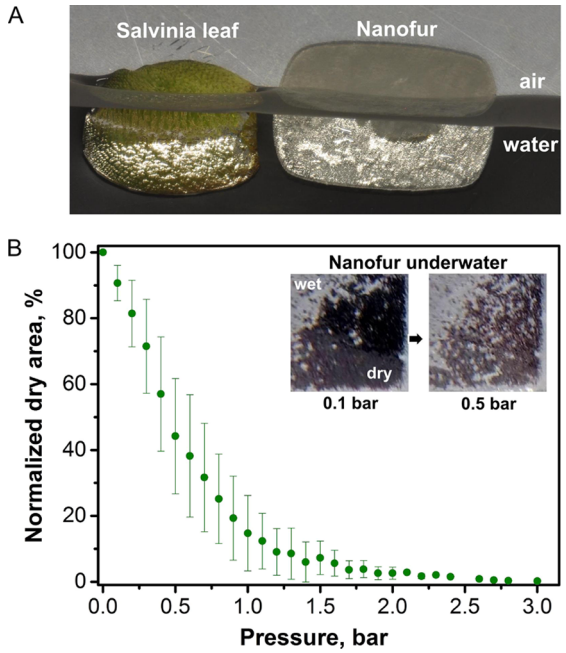

Figure 2. (A) Optical image of the nanofur and *Salvinia Molesta* leaf partially submerged underwater. Silvery layers visible on both surfaces indicate the trapped air layer, and are the result of light reflection from the interface between the trapped air and water. (B) Measured average normalized nanofur area covered by air (dry area) as a function of applied pressure. Image processing of consecutive images of ten nanofur samples taken at different pressures was used to obtain the data. The error bars represent standard deviation. The processed images (tilt-corrected) from a typical measurement on the nanofur at two different pressures can be seen in the inset. The area covered by air appears dark in the images, while the wet area is light.

insects, identified surface characteristics important for stable long-term air retention, which include hydrophobicity, micro- to millimeter-long hairs, additional finer structures such as nanohairs, micro- and nanocavities, and elasticity of the structures. These identified criteria are satisfied by the surface of the nanofur. The nanofur is able to retain a stable air layer underwater for more than 31 days, as was previously observed by studying the intensity profiles of the air/water interface using confocal microscopy.[24] After 31 days, the experiment was stopped with the air film still present. As comparison, on the water fern *Salvinia*, the air layer is stable for up to 17 days,[21] and on the upper surface of the water bug for more than 130 days.[9]

To investigate the robustness of the underwater air film on the irregular surface topography of the nanufur, we analyzed the air−water interface above nanofur underwater at different applied pressures. The nanofur surface underwater is shimmering (Figure 2A), but when the air layer is replaced by water under external pressure, the surface looses its superhydrophobicity (transition from Cassie−Baxter to Wenzel wetting state) and becomes opaque. In this experiment a 1 cm × 1 cm nanofur sample (N = 10) was placed vertically into a transparent container filled with deionized water (head of water is 3.5 cm) and at an angle to the camera. The container was sealed, and the pressure inside was slowly increased using compressed air, and monitored using a gauge pressure sensor. To improve the visibility of the underwater air layer, a black background was installed next to the container which made the reflecting air−water interface appear dark. A collapse of the

DOI: 10.1021/acsami.5b01772
ACS Appl. Mater. Interfaces 2015, 7, 10651−10655

air−water interface on the surface was observed by the change of color from dark to light, due to reduced reflectivity of the collapsed areas. Consecutive images of the superhydrophobic nanofur underwater were taken at different applied pressures. The images were tilt-corrected, converted to grayscale, and a threshold was applied to extract the percentage of dry area covered by air at each pressure. The processed images from a typical measurement on the nanofur at two different pressures can be seen in the inset of Figure 2B. To estimate the error introduced by the tilt-correction procedure, we processed the tilted and not tilted images of graph paper samples (N = 3) using the same procedure, and the estimated difference is less than 1%.

The measured nanofur surface area covered by air (dry area) at each applied pressure was normalized to the measured dry area with no external pressure applied for each sample to allow the direct comparison of different samples. The resulting average normalized dry area as a function of pressure was measured on ten different nanofur samples and is shown in Figure 2B. The error bars represent the standard deviation. The dry area exponentially decreases with the applied pressure. 50% of the initial air layer retained by nanofur is stable under pressure ∼0.5 bar, and 10% at ∼1.4 bar. The stability of the air layer in Salvinia plants was recently studied by Mayser and Barthlott.[18] In *Salivinia molesta* the first water penetration between the eggbeater-shaped hairs occurs at ∼0.12 bar, and at 3.6 bar most of the air is replaced with water. The lotus leaf can sustain the air layer only below 0.135 bar.[28]

Next we compare experimental results with the theoretically predicted critical applied pressure (P_{cr}) for the nanofur topography. P_{cr} is the pressure required to break the air−water interface and, therefore, allow water to infiltrate the space between nano- and microhairs and wet the surface. The model for nanofur description is chosen considering its fabrication procedure, in which a rough hot sandblasted plate forms microcavities surrounded by hairs (inset in Figure 3). Assuming that the cavities are not interconnected, the nanofur surface is described as composed of circular pores with the same diameter. The diameter of the blasting particles used to fabricate the sandblasted plate is 53 μm, and is used as the pore diameter. The thickness (depth) of the nanofur layer is 56 ± 19 μm as determined from cross-sectional SEM images (Figure 1B). Based on the work of Hemeda et al. the air−water interface above the surface consisting of circular pores is described as spherical caps, and P_{cr} is calculated using a balance of forces which considers hydrostatic, ambient, capillary and the entrapped air pressures.[29] The calculated P_{cr} required to break the air−water interface above the nanofur cavities is 0.43 bar (for θ = 174°). The dependence of P_{cr} on pore diameter and depth is plotted in Figure 3. The shaded area in the graph describes theoretical P_{cr} for the measured nanofur depth and its standard deviation. The theoretically calculated P_{cr} is in agreement with experimentally measured data (Figure 2B). Moreover, the gradual decrease in the experimentally measured area covered by air is a result of the nanofur topography consisting of different size microcavities, and thus having different P_{cr}.

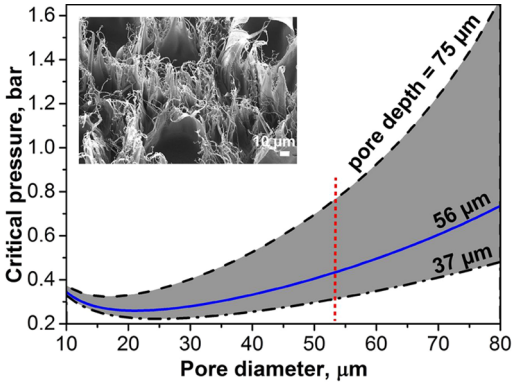

Figure 3. Theoretical critical pressure P_{cr} for the nanofur surface composed of circular pores (microcavities) as a function of pore diameter and depth. The shaded area in the graph is P_{cr} for the measured nanofur pore depth (56 ± 19 μm), and the highlighted pore diameter (53 μm) is the diameter of the nanofur pores. The pore-based model for nanofur description is chosen considering its fabrication procedure, in which a rough hot sandblasted plate forms microcavities surrounded by hairs (SEM image in the inset).

Water on the nanofur surface rests on the tips of the nanohairs with air pockets sealed between them, forming the Cassie−Baxter wetting state and a composite polycarbonate-air−water interface.[19] Therefore, the fluid velocity at the tips of the nanohairs (water−polycarbonate contact area) matches the velocity at the surface, implying that the no-slip boundary condition applies to these areas as to other flat surfaces (Figure 4A). In contrast, on the shear-free water−air interface the no-slip boundary condition is no longer applicable, resulting in the maximum velocity at this interface.[7] The velocity profile on the superhydrophobic nanofur surface consisting of hairs and air pockets on which fluid experiences slip and nonzero velocity at the surface is shown in Figure 4B. The presence of air pockets on the surface results in reduction of the solid surface area in contact with water, which in turn leads to frictional drag reduction.

To study the fluid drag reduction properties of the nanofur, we measured and compared the pressure drops resulting from the water flow across channels with walls made from nanofur and flat polycarbonate (PC). Nanofur and flat PC sheets were used as bottom wall surfaces of the rectangular channel. To fabricate the closed channel system, the top channel structure was first fabricated using PDMS (Sylgard 184), and then the nanofur or flat PC was inserted into the bottom of the PDMS channel. The channel was sealed using silicone adhesive, clamped between two Plexiglas panels, and purged to remove any air bubbles trapped inside. The dimensions of the resulting channel are 40 mm × 6 mm × 0.5 mm (length × width × height). The water flow in the channel was generated with a pump (Ismatec, Germany). The pressure drop across the channel was measured using two tubes inserted at its inlet and outlet (center-to-center distance is 30 mm). The recorded water level difference between the tubes and the Bernoulli principle were used to calculate the pressure drop in the channel. A schematic of the experimental setup for measuring pressure drop is shown in Figure 4C. Reynolds number was calculated as

$$Re = \frac{cD_h}{\nu} \quad (1)$$

where c is the flow velocity obtained from the experimental volumetric flow rate divided by the channel cross-section, ν is the kinematic fluid viscosity, and D_h is the hydraulic diameter of the channel, calculated as $D_h = 2\,w\,h/(w+h)$ for rectangular channel with width w and height h.[30]

DOI: 10.1021/acsami.5b01772
ACS Appl. Mater. Interfaces 2015, 7, 10651−10655

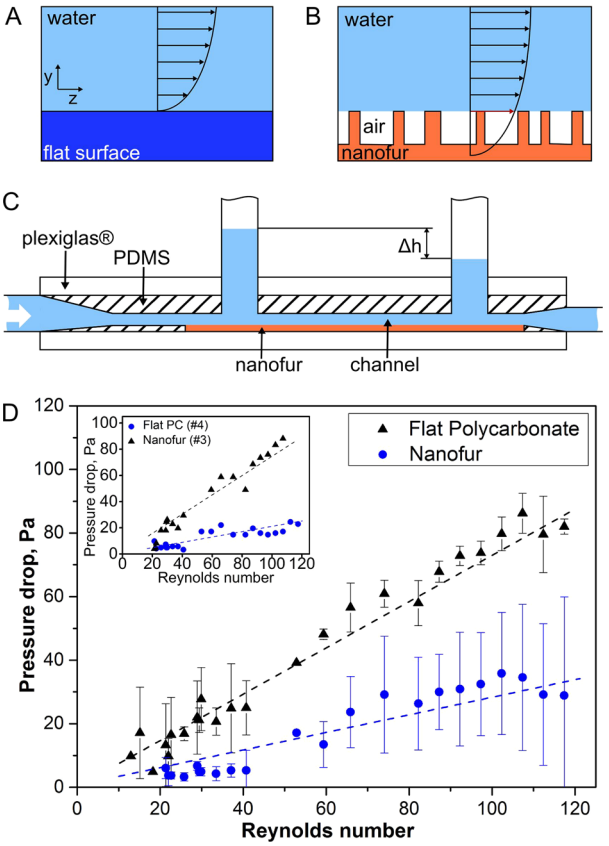

Figure 4. (A) Fluid velocity profile at the surface with no-slip boundary condition. The velocity at the surface is zero. (B) Velocity profile on the superhydrophobic nanofur surface consisting of hairs and air pockets. Fluid experiences slip and nonzero velocity at the surface (red arrow). (C) Cross-sectional schematic of the experimental setup used for measuring the pressure drop across the microchannels. The nanofur or flat PC are inserted into the bottom of the microchannel. (D) Experimental pressure drop in the microchannels with nanofur wall and with flat polycarbonate (PC) wall as a function of the Reynolds number. The average pressure drop values represent measurements from four independent microchannels with each wall type. The lower pressure drop for the channels with nanofur indicates the reduced fluid drag resulting from the retained air layer. The error bars represent the 95% confidence interval of the mean. The dashed lines are a guide to the eyes. Typical measurements from two channels with different walls are shown in the inset.

The average pressure drop measured in the channels with and without the nanofur wall is shown as a function of the Reynolds number in Figure 4D. Four microchannels with unique surfaces of each type were used to obtain the data. The error bars represent the 95% confidence interval of the mean. The typical measurements from two channels with different walls are shown in the inset in Figure 4D. In the tested range of Reynolds numbers, the measured pressure drop across the channels lined with nanofur is approximately 50% lower than in the channels lined with unstructured polymer. Lower pressure drop for the nanofur indicates the reduction in fluid drag by the material, resulting from the air layer retained on its nano- and microstructured surface.

In conclusion, we investigated the properties of the superhydrophobic bioinspired nanofur material with irregular surface topography. Nanofur is fabricated using a highly scalable hot pulling technique, in which the main tool is a heated sandblasted steel plate. The resulting nanofur is covered by a layer of randomly distributed high aspect ratio nano- and microhairs, analogous to the natural model air-retaining surfaces. We studied the stability of the underwater air layer retained by the nanofur by applying different hydraulic pressures to the nanofur kept underwater. Our results revealed the gradual collapsing of the air layer retained by the nanofur, with 50% of the initial layer stable at ∼0.5 bar, and 10% at ∼1.4 bar. Thus, the stability of the air layer retained on the nanofur surface is comparable to *Salvinia* surface, and is higher than the Lotus leaf surface. Additionally, theoretically predicted critical pressures for the nanofur are in agreement with experiment. Furthermore, we evaluated the drag reduction properties resulting from the nanofur air-retention. We measured the pressure drop across channels in which the nanofur served as a channel wall, and compared it to channels with flat walls. We observed that in the tested range of Reynolds numbers, the pressure drop across the nanofur channels with nanofur is approximately 50% lower than in the channels with the unstructured surface, indicating that drag reduction occurred.

AUTHOR INFORMATION

Corresponding Authors

*E-mail: maryna.kavalenka@kit.edu.
*E-mail: hendrik.hoelscher@kit.edu.

Notes

The authors declare no competing financial interest.

ACKNOWLEDGMENTS

The authors thank Paul Abaffy for help with SEM images, and Botanical Gardens of the University of Bonn for providing *Salvinia* plants. This work was partly carried out with the support of the Carl Zeiss Foundation, Landesgraduiertenförderung, and the Karlsruhe Nano Micro Facility (KNMF, www.kit.edu/knmf), a Helmholtz Research Infrastructure at Karlsruhe Institute of Technology (KIT, www.kit.edu).

REFERENCES

(1) Tao, P.; Shang, W.; Song, C.; Shen, Q.; Zhang, F.; Luo, Z.; Yi, N.; Zhang, D.; Deng, T. Bioinspired Engineering of Thermal Materials. *Adv. Mater.* **2015**, *27*, 428463.
(2) Wang, J.; Liu, M.; Ma, R.; Wang, Q.; Jiang, L. In Situ Wetting State Transition on Micro- and Nanostructured Surfaces at High Temperature. *ACS Appl. Mater. Interfaces* **2014**, *6*, 15198−15208.
(3) Zhao, N.; et al. Bioinspired Materials: from Low to High Dimensional Structure. *Adv. Mater.* **2014**, *26*, 6994−7017.
(4) Wegst, U. G. K.; Bai, H.; Saiz, E.; Tomsia, A. P.; Ritchie, R. O. Bioinspired Structural Materials. *Nat. Mater.* **2015**, *14*, 23−36.
(5) Eyring, V.; Köhler, H. W.; van Aardenne, J.; Lauer, A. Emissions from International Shipping: 1. The Last 50 Years. *J. Geophys. Res. Atmos.* **2005**, *110*, D17305.
(6) Wang, J.; Lan, S.; Chen, G. Experimental Study on the Turbulent Boundary Layer Flow over Riblets Surface. *Fluid Dyn. Res.* **2000**, *27*, 217−229.
(7) McHale, G.; Newton, M.; Shirtcliffe, N. Immersed Superhydrophobic Surfaces: Gas Exchange, Slip and Drag Reduction Properties. *Soft Matter* **2010**, *6*, 714−719.
(8) Gao, X.; Jiang, L. Biophysics: Water-Repellent Legs of Water Striders. *Nature* **2004**, *432*, 36.
(9) Ditsche-Kuru, P.; Schneider, E. S.; Melskotte, J.-E.; Brede, M.; Leder, A.; Barthlott, W. Superhydrophobic Surfaces of the Water Bug Notonecta glauca: a Model for Friction Reduction and Air Retention. *Beilstein J. Nanotechnol.* **2011**, *2*, 137−144.
(10) Zhao, J.; Zhang, X.; Chen, N.; Pan, Q. Why Superhydrophobicity Is Crucial for a Water-Jumping Microrobot?

DOI: 10.1021/acsami.5b01772
ACS Appl. Mater. Interfaces 2015, 7, 10651−10655

Experimental and Theoretical Investigations. *ACS Appl. Mater. Interfaces* **2012**, *4*, 3706−3711.
(11) Barthlott, W.; Schimmel, T.; Wiersch, S.; Koch, K.; Brede, M.; Barczewski, M.; Walheim, S.; Weis, A.; Kaltenmaier, A.; Leder, A.; Bohn, H. F. The Salvinia Paradox: Superhydrophobic Surfaces with Hydrophilic Pins for Air Retention under Water. *Adv. Mater.* **2010**, *22*, 2325−2328.
(12) Ou, J.; Perot, B.; Rothstein, J. Laminar Drag Reduction in Microchannels Using Ultrahydrophobic Surfaces. *Phys. Fluids* **2004**, *16*, 4635−4643.
(13) Shirtcliffe, N.; McHale, G.; Newton, M.; Zhang, Y. Superhydrophobic Copper Tubes with Possible Flow Enhancement and Drag Reduction. *ACS Appl. Mater. Interfaces* **2009**, *1*, 1316−1323.
(14) Balasubramanian, A.; Miller, A.; Rediniotis, O. Microstructured Hydrophobic Skin for Hydrodynamic Drag Reduction. *AIAA J.* **2004**, *42*−*2*, 442−451.
(15) Gogolides, E.; Ellinas, K.; Tserepi, A. Hierarchical Micro and Nano Structured, Hydrophilic, Superhydrophobic and Superoleophobic Surfaces Incorporated in Microfluidics, Microarrays and Lab on Chip Microsystems. *Microelectron. Eng.* **2015**, *132*, 135−155.
(16) Srinivasan, S.; Kleingartner, J.; Gilbert, J.; Cohen, R.; Milne, A.; McKinley, G. H. Sustainable Drag Reduction in Turbulent Taylor-Couette Flows by Depositing Sprayable Superhydrophobic Surfaces. *Phys. Rev. Lett.* **2015**, *114*, 014501.
(17) Papadopoulos, P.; Mammen, L.; Deng, X.; Vollmer, D.; Butt, H.-J. How Superhydrophobicity Breaks Down. *Proc. Natl. Acad. Sci. U.S.A.* **2013**, *110*, 3254−3258.
(18) Mayser, M.; Barthlott, W. Layers of Air in the Water beneath the Floating Fern Salvinia are Exposed to Fluctuations in Pressure. *Integr. Comp. Biol.* **2014**, *54*, 1001−1007.
(19) Tuvshindorj, U.; Yildirim, A.; Ozturk, F.; Bayindir, M. Robust Cassie State of Wetting in Transparent Superhydrophobic Coatings. *ACS Appl. Mater. Interfaces* **2014**, *6*, 9680−9688.
(20) Balmert, A.; Bohn, H. F.; Ditsche-Kuru, P.; Barthlott, W. Dry under Water: Comparative Morphology and Functional Aspects of Air-Retaining Insect Surfaces. *J. Morphol.* **2011**, *272*, 442−451.
(21) Koch, K.; Barthlott, W. Superhydrophobic and Superhydrophilic Plant Surfaces: an Inspiration for Biomimetic Materials. *Philos. Trans. R. Soc., A* **2009**, *367*, 1487−1509.
(22) Solga, A.; Cerman, Z.; Striffler, B.; Spaeth, M.; Barthlott, W. The Dream of Staying Clean: Lotus and Biomimetic Surfaces. *Bioinspiration Biomimetics* **2007**, *2*, 126−134.
(23) Röhrig, M.; Schneider, M.; Etienne, G.; Oulhadj, F.; Pfannes, F.; Kolew, A.; Worgull, M.; Hölscher, H. Hot Pulling and Embossing of Hierarchical Nano- and Micro-Structures. *J. Micromech. Microeng.* **2013**, *23*, 105014.
(24) Röhrig, M.; Mail, M.; Schneider, M.; Louvin, H.; Hopf, A.; Schimmel, T.; Worgull, M.; Hölscher, H. Nanofur for Biomimetic Applications. *Adv. Mater. Interfaces* **2014**, *1*, 1300083.
(25) Worgull, M. *Hot Embossing−Theory and Technology of Micro Replication*; William Andrew: Oxford, U.K., 2009.
(26) Kavalenka, M. N.; Hopf, A.; Schneider, M.; Worgull, M.; Hölscher, H. Wood-Based Microhaired Superhydrophobic and Underwater Superoleophobic Surfaces for Oil/Water Separation. *RSC Adv.* **2014**, *4*, 31079−31083.
(27) Worgull, M.; Schneider, M.; Röhrig, M.; Meier, T.; Heilig, M.; Kolew, A.; Feit, K.; Hölscher, H.; Leuthold, J. Nanoimprinting and Thermoforming of Biodegradable Three-Dimensional Wood Structures. *RSC Adv.* **2013**, *3*, 20060−20064.
(28) Sheng, X.; Zhang, J. Air Layer on Superhydrophobic Surface Underwater. *Colloids Surf., A* **2011**, *377*, 374−378.
(29) Hemeda, A.; Tafreshi, H. V. General Formulations for Predicting Longevity of Submerged Superhydrophobic Surfaces Composed of Pores or Posts. *Langmuir* **2014**, *30*, 10317−10327.
(30) Jung, Y.; Bhushan, B. Biomimetic Structures for Fluid Drag Reduction in Laminar and Turbulent Flows. *J. Phys.: Condens. Matter* **2010**, *22*, 035104.

DOI: 10.1021/acsami.5b01772
ACS Appl. Mater. Interfaces 2015, 7, 10651−10655